ELSEVIER

Physica B 253 (1998) 203–214

PHYSICA B

Study on bound exciton dynamics in CdS crystals at acoustic driving

O.A. Korotchenkov*,[1], T. Goto

Department of Physics, Graduate School of Science, Tohoku University, Sendai 980, Japan

Received 11 December 1997; received in revised form 3 March 1998

Abstract

A variety of ps transient and cw optical techniques including photoluminescence (PL), Raman scattering and optical absorption spectroscopy has been applied to elucidate acoustically driven bound exciton dynamics. The lifetime of the I_1 bound excitons in CdS platelets is found to be initially enhanced with increasing driving amplitude whereas a drop in the lifetime is achieved at sufficiently high drivings. The line shape of the I_1 exciton PL lines experiences remarkable broadening in the region of the lifetime decrease and this is accompanied by a reduced light emission in the acoustic phonon wing of the I_1 exciton PL line. Additionally, an enhancement of the E_1 LO phonon resonant Raman line and an appearance of the A_1 LO phonon Raman line, normally forbidden in the employed scattering geometry, are achieved by increasing the driving amplitude. The detailed analysis of the observations is made within the framework of internal electric fields generated by the driving. It is shown that the effects presented can be reasonably well understood by taking into account both the long-range electric fields and nonuniform microfields accompanying acoustic driving. It is shown that the microfields likely arise from variations in the local-crystal environment at the exciton site imposed by the driving. © 1998 Elsevier Science B.V. All rights reserved.

PACS: 71.35. −y; 71.55. −i; 63.20. −e

Keywords: CdS; Acoustic driving; Excitons; Photoluminescence; Raman scattering

1. Introduction

The near-band-edge photoluminescence (PL) of direct gap III–V and II–VI semiconductors is usually dominated at low temperatures by excitonic transitions. Among the attractive excitonic properties of these materials are bound exciton complexes which are known to exhibit very narrow PL lines and considerably obscure the intrinsic free-exciton transitions. It is widely accepted that this narrowness comes from the fact that the electron–hole pair is strongly localized around the binding center [1] although its quantitative description and exciton–phonon broadening mechanisms are as yet a matter of active research work [2,3].

* Corresponding author. Tel.: + 81 22 217 6422; fax: + 81 22 217 6498; e-mail: olegk@mail.cc.tohoku.ac.jp.

[1] Permanent address: Faculty of Physics, Kiev University, Kiev 252022, Ukraine, Russian Federation.

0921-4526/98/$ – see front matter © 1998 Elsevier Science B.V. All rights reserved.
PII: S0921-4526(98)00390-1

The bound exciton PL lines have been of continuous interest for a long time and various applications has been reported such as control of a crystal purity at its growth, determination of impurity contents [4], optical gain and laser emission with excitonic states in II–VI semiconductor structures [5], etc.

One of the important quantities for an understanding of the dynamics of photoexcited carriers in semiconductors which are particularly influenced by excitonic effects is the oscillator strength or the lifetime of a radiative transition. Application of external parameters, particularly, electric fields is known to affect the exciton dynamics in semiconductors and semiconductor structures. An electric field-induced increase of the recombination lifetime has been observed in quantum wells due to the polarization of electron–hole pairs [6]. The strong piezoelectric field of a surface acoustic wave in a quantum well structure has been shown to spatially separate photogenerated electron–hole pairs which dramatically reduces recombination probabilities and increases the radiative lifetimes by several orders of magnitude [7]. It has been found that electric fields accompanying acoustic waves in bulk materials have a profound influence on the PL intensity of bound excitons [8]. The principal possibility of a lifetime tuning in a binding excitonic system due to electric fields accompanying acoustic waves has also been demonstrated [9]. A remarkable dislocation-mediated quenching effect on excitonic luminescence has been achieved in CdS crystals [10]. It is worth noting that internal electric fields as high as 10^5 V/cm have been observed in CdS crystals due to the effects of moving charged dislocations [11].

The aim of the present work is to study the effects of acoustic driving on bound exciton dynamics in CdS crystals subjected to MHz-frequency vibrations. It is shown that the radiative transitions on bound excitons and Raman scattering resonant with the bound exciton state can be effectively varied by the driving and the tentative mechanism of the effects is offered. We believe that the ideas of acoustic driving on the exciton dynamics could have particular optoelectronic applications and seem worth extending.

2. Experiment

A number of undoped CdS single-crystal platelets grown from the vapour phase which appeared to be insulating in the dark were used in experiments. All the investigated samples displayed essentially similar effects, although the size of the effect was found to vary with the sample used. The data presented below were taken with the sample with a thickness of about 400 μm and linear dimensions close to 4.8×7.2 mm^2. In this work, care was exercised to ensure a highest optical quality of the platelet so that not any sample surface treatment was introduced. Accordingly, the shape of the sample was not perfect, thus tremendously complicating the analysis of the sample vibrational modes, as will be seen below.

Acoustic driving in a piezoelectric CdS crystal 1 was introduced by applying an RF voltage U to the metal electrodes 2 deposited on the edge of the opposite crystal surfaces, as sketched in Fig. 1. Similar electrodes 3 were used in order to detect the vibrational response. The sample was mounted to a copper bar which served as the electrical ground connection. No bond was used between the crystal and the bar. The sample was slightly held down by two stainless steel springs which were attached to the upper electrodes 2 and 3 and connected to an RF signal. The sample was then cooled in a liquid helium bath cryostat.

The sample temperature was controlled by a carbon-glass resistor attached to the bar close to the sample surface. No sample heating was detected in the range of driving voltages and frequencies employed in the work. It should also be mentioned that any possible thermal effect of acoustic driving can be ruled out by analyzing the data presented below.

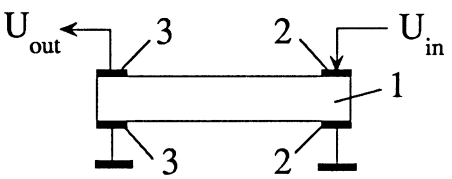

Fig. 1. Schematic of the experimental setup, showing CdS platelet (1) and metal electrodes (2, 3).

Polarized PL and Raman scattering measurements in almost backscattering geometry were carried out at 4.2 K using a T64000 Jobin–Yvon monochromator with a CCD detector and an argon laser. All the spectra presented here were taken with light traveling and polarized perpendicular to the c axis of CdS. In order to estimate internal electric fields in the platelets, a shift of the absorption edge to a lower energy upon increasing U was detected with a SpectraPro-500 monochromator and a tungsten lamp. The lamp illumination was properly suppressed to ensure minimum amount of light in transmission experiments. Previous transmission experiments performed on ZnS and CdS crystals tested this technique for diagnosing electric fields generated by acoustic driving [12]. Light from a crystal was focused onto the entrance slit of a monochromator by a lens with a 127 mm focus length such that the sample image was enlarged compared to the sample size. This was done in order to detect emissions from the central part of the sample surface and to eliminate the possible influence of the sample edges and near electrode areas of the platelet on the optical spectra.

For the emission decay measurements, picosecond laser pulses of about 1 meV spectral width were obtained from a tunable Ar^+ pumped Ti:sapphire laser operating with a 76 MHz repetition rate and equipped with a $LiIO_3$ nonlinear crystal. The spectral position of the laser was tuned to 4880 Å. A subtractive double monochromator with a reciprocal dispersion of 0.7 nm/mm and a Hamamatsu C-5680 streak camera were employed in this measurement. The power density was set at 0.15 W/cm^2 for the cw excitation and at 0.05 W/cm^2 on an average for the pulse excitation.

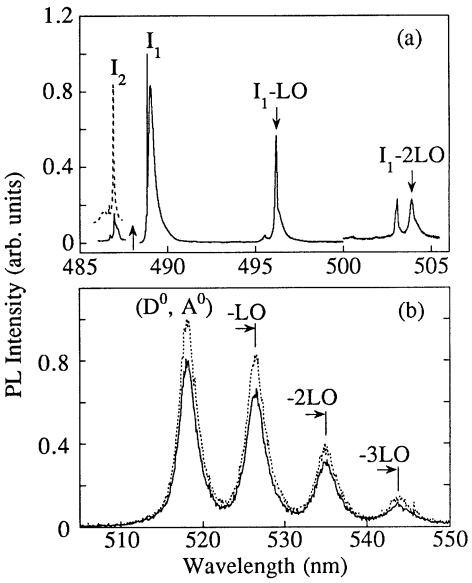

Fig. 2. PL spectra of the CdS platelet taken at 4.2 K. Solid curves in panel (a) show the I_1 and I_2 lines along with the longitudinal optical phonon replicas I_1–LO and I_1–2LO of the I_1 line excited with the 4880 Å line of an argon laser (an upward arrow). The I_2 solid line is recorded as anti-Stokes luminescence and is 5 times magnified in the figure compared to the I_1 and I_1–LO lines. The intensities of the I_1–LO and I_1–2LO lines are in the ratio 1 : 0.12, respectively. 2LO Raman scattering line is seen on the left side of the I_1–2LO emission line whereas the LO Raman line is not clearly resolved in the spectrum because of its relative weakness. The dashed curve represents the I_2 emission line taken with the 4765 Å line of an argon laser and it is in an arbitrary scale. Solid curve in panel (b) represents the set of edge-luminescence bands which corresponds to the donor-to-acceptor recombination at about 518 nm [13] successively separated by the LO phonon energy. The dotted line demonstrates an enhanced edge emission at $U = 72$ V accompanying the quenching of the exciton PL lines (see text).

3. Results

The photoluminescence spectrum of our sample is shown in Fig. 2. The I_1 line in Fig. 2a is the decay of an exciton bound to a neutral acceptor and the I_2 line corresponds to an exciton bound to a neutral donor [13]. An edge emission band at about 518 nm was successively separated by a set of the LO phonon shifted lines as Fig. 2b illustrates. This emission is due to the radiative recombination of an electron bound to an ionized donor, D^+, and a hole bound to an ionized acceptor, A^-, i.e., the donor-to-acceptor, (D^0, A^0) recombination [14]. The data presented below are taken with the I_1 transition excited with the 4880 Å laser line which is higher in energy than the I_1 line (4888 Å) as seen in Fig. 2a, but well below the band gap of CdS (4802 Å at 4.2 K) thus considerably suppressing possible thermal effects originating from free carriers.

The excitonic PL lines in Fig. 2a appear to be sharp and well-formed. It is therefore, unlikely that a uniform crystal stress was introduced by the setup

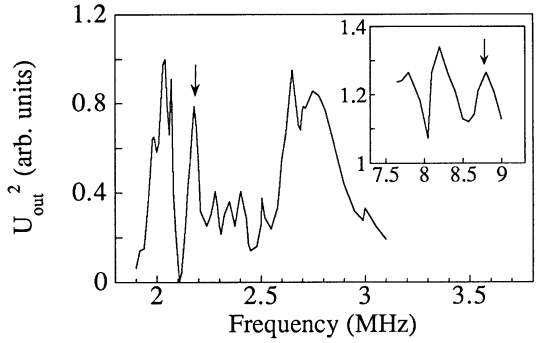

Fig. 3. The transmitting vibrational response of the CdS platelet detected by the output RF signal in the experimental arrangement depicted in Fig. 1. Arrow in the figure indicates the frequency of the first thickness resonance of the platelet estimated from Eq. (1) while that in the inset corresponds to the computed frequency of the fifth thickness eigenmode of the plate vibrations.

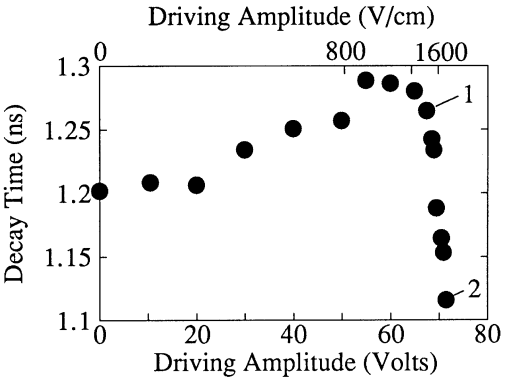

Fig. 4. Lifetime dependence of the I_1 emission line presented in Fig. 2a for various driving amplitudes.

which is designed with the mechanical load on the sample surfaces being minimized. However, the resonant response of the platelet presented in Fig. 3 exhibits rather complicated mode behaviors. It is instructive to note in this respect that an accurate identification of the vibrational modes requires to take into account a number of critical parameters [15]. First of all, the shape of the sample would be well defined which is not the case in our studies as already pointed out. Further, the mounting of the sample would ideally not affect the sample resonances which is obviously not satisfied in our sample arrangement. Hence, an unambiguous identification of platelet modes seems unlikely to be made with the data presented in Fig. 3. Meanwhile, we attempted to identify the frequencies of the thickness vibrational modes from

$$f_{l,t}^{n} = n(v_{l,t}/2d), \tag{1}$$

where $v_{l,t}$ the velocity of either the longitudinal (l) or the transverse (t) acoustic wave in CdS, d is the thickness of a platelet, and $n = 1, 2, 3, \ldots$. The results of the estimates for the first and fifth thickness vibrational modes shown by arrows in Fig. 3 and in the inset of Fig. 3, respectively, verify that such modes are likely excited in our sample. However, the presented assignment is subject to the concerns about the nonuniform spacing of the frequencies f^n in the piezoelectric resonator and to the nonperfect shape of our sample such that an identification of vibrational modes of the platelet is beyond the purposes of the present study.

We report here the data taken from the CdS platelet driven at frequencies from 8 to 9 MHz. No frequency-dependent effects on the exciton dynamics have been developed in this study and only the size of the observed effects has varied with the driving frequency.

The decay time of the I_1 exciton PL line with increasing driving amplitude is shown in Fig. 4. It is initially enhanced at low driving amplitudes below $U \approx 60$ V, whereas a drop in the decay time is achieved in the region $60\ \mathrm{V} \leqslant U \leqslant 70$ V. Two original traces of a streak camera which correspond to points 1 and 2 in Fig. 4 are exemplified in Fig. 5. The experimental points presented in Fig. 4 have been obtained from the slopes of decay curves similar to that shown in Fig. 5. At sufficiently low temperatures, the decay time of bound excitons is commonly believed to be their true lifetime. Therefore, the data presented in Fig. 4 indicate acoustically driven changes in the I_1 exciton lifetime.

In spite of remarkable changes of the I_1 exciton PL line shapes accompanying observed decrease of the decay time (spectra 3 in Fig. 6a and b), the total integrated luminescence intensity of the I_1 lines is not changed appreciably in the chosen driving range as evidenced by the data in Fig. 7. Hence the

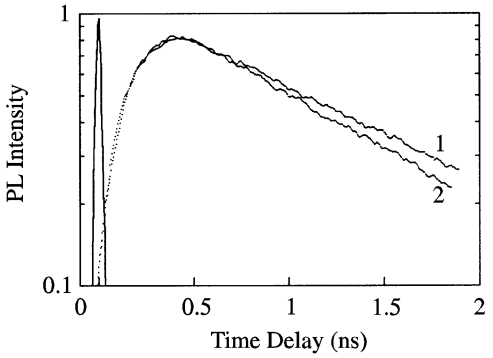

Fig. 5. Decay curves of the I_1 emission line at two driving amplitudes (points) normalized to their maxima. The points 1 and 2 in Fig. 4 are taken from the slopes of the curves 1 and 2 in Fig. 5. The laser excitation pulse is shown by the solid curve.

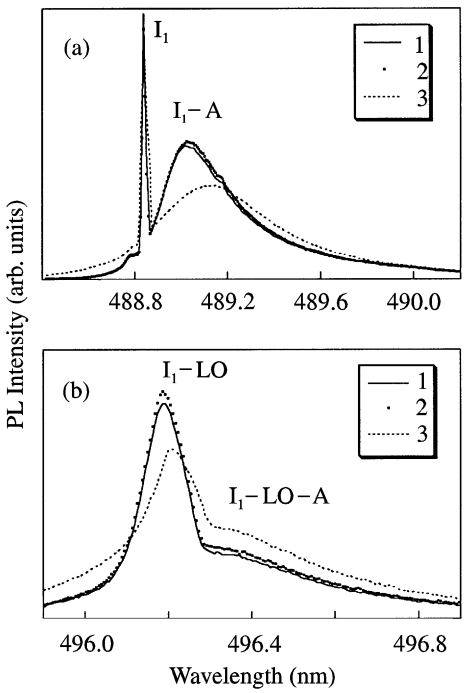

Fig. 6. Evolution of the I_1 line, its acoustic phonon replica I_1–A and its LO phonon replica I_1–LO accompanied by acoustic phonon wing I_1–LO–A with increasing driving amplitude: $U = 0$ (1), 60 V (2) and 70 V (3).

influence of nonradiative processes on the exciton lifetimes presented in Fig. 4 is small. Upon increasing U above ≈ 70 V, quenching of the I_1 emission lines has appeared (downward arrow in Fig. 7) and

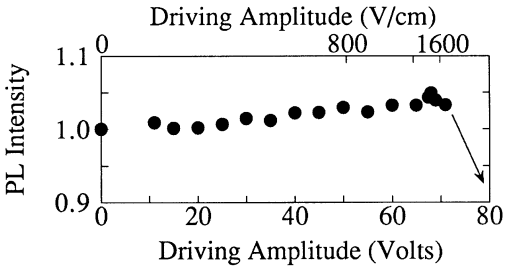

Fig. 7. The integrated emission intensity in the I_1 lines as a function of the driving amplitude.

it is accompanied by an increase in the (D^0, A^0) emission (dotted curve in Fig. 2b).

4. Discussion

We start our discussion from the fact that the I_1 exciton PL intensities are suppressed by the driving above $U \approx 70$ V. Possible explanations attempted for the observed suppression of exciton luminescence fall into three main physical mechanisms: (i) thermal dissociation; (ii) driven-induced enhancement of the nonradiative transitions; (iii) ionization in electric fields accompanying acoustic waves in a piezoelectric CdS.

As noted earlier, no sample surface temperature increase has been detected. Moreover, it is also worth noting that the lifetime of the bound excitons taken at about 4 K is expected to be independent of temperature. Only the decrease of the luminescence intensity is anticipated with increasing temperature because of ionization of the bound excitons. No such PL intensity decrease is seen in Fig. 7 below $U \approx 70$ V, thus providing additional proof against possible thermal effects in the chosen driving range. It is therefore not unreasonable to assume that thermal dissociation (i) does not constitute the exciton quenching mechanism.

Besides radiative decay, bound excitons can decay nonradiatively and there exists an abundant evidence demonstrating that the nonradiative recombination of bound excitons through an Auger process is highly probable. In the Auger effect, an electron and hole of the I_1 exciton bound to a neutral acceptor recombine and the energy of the

bound exciton is transferred to the hole on the acceptor which is ejected from the impurity atom. However, the explanation (ii) is inconsistent with the observation of an enhanced donor-to-acceptor emission in Fig. 2b accompanying the effect on bound excitons. This enhancement likely signifies an increased free carrier concentration in the conduction and valence bands since the capture probability of charged carriers dissociated from bound excitons by ionized donors D^+ and acceptors A^- with a subsequent (D^0, A^0) recombination has been found to be remarkably high [16].

We therefore interpret our data by showing that electric fields accompanying the driving would suppress the exciton luminescence above $U \approx 70$ V, as shown by the downward arrow in Fig. 7, and affect the I_1 exciton emission decay time and line shapes below this driving limit, as seen in Figs. 4 and 6. To attain the electric field strengths, optical absorption measurements have been performed.

Absorption spectra of the platelet are presented in Fig. 8. Spectrum 1 exhibits an absorption edge with a weak exciton series. These excitons have lower binding energies than those of the I_1 exciton and can be identified as the I_{1B} (peak a in Fig. 8), I_3 (peak b), Y (peak c) and E_A (peak d) excitons in the notations introduced by Thomas and Hopfield [13]. An influence of acoustic driving has appeared as a shift of the edge to lower energies with accompanying blurring of the exciton series (2 in Fig. 8). The effect of acoustic waves on the intensity of excitonic transitions in CdS crystals has been

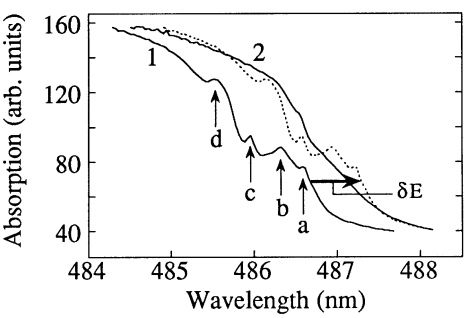

Fig. 8. Absorption edge of the sample at $U = 0$ (1) and $U = 70$ V (2). The dashed curve is the spectrum 1 shifted $\delta E = 3.26$ meV to lower energy which estimates an electric field $F \approx 1.6$ kV/cm by Eq. (2).

reported in the literature [10] so that the blurring of the exciton series in Fig. 8 will not be further discussed here. For the purposes of the present study, it is essential to emphasize that the observed shift of the absorption edge allows a rough estimate of internal electric fields generated by the driving [12]. The conversion of externally applied voltage U into electric field F inside the crystal has been done by fitting the energy shift δE of the absorption edge in Fig. 8 to the Eq. [17]

$$\delta E = (3/2m^{*1/3})(e\hbar F)^{2/3}, \quad (2)$$

where $m^* = 0.141m_0$ [18] is the reduced interband effective mass, e and m_0 are the electron charge and mass, respectively, and $\hbar$ is the Planck's constant.

The upper scales in Figs. 4 and 7 have been obtained by such a fitting. Its reliability can be checked by a simple dimensional estimate within the framework of impact ionization of excitons which is known to cause the exciton quenching in II–VI compounds by electric field [19]. By attributing the energy $m^*\mu^2F^2/2$ gained by free electrons with the mobility $\mu \approx 3 \times 10^4$ cm^2 V/s [20] from the field F to the dissociation energy of the I_1 exciton which is taken to be 50 meV, the resulting ionization threshold is about 1100 V/cm. The threshold value of the order of 1600 V/cm deduced from Fig. 7 at $U \approx 70$ V is somewhat higher. However, taking into account the crude assumptions made, this may be considered as reasonably good agreement.

Therefore, the field scales introduced in Figs. 4 and 7 can serve at best as a rough approximation to the internal electric fields generated by acoustic driving. It has to be mentioned that some ambiguity about the definition of the field arises from the fact that CdS platelets have been shown to be subject to acoustically induced changes of the net charge at crystal defects [21]. The net charge depends very strongly on the driving amplitude, and the generated electric field can in general not be proportional to the driving amplitude as is the case experimentally in Figs. 4 and 7. For the purposes of the present study, we distinguish between long-range electric fields generated by the driving and short-range microfields exerted by externally driven lattice vibrations. When it comes to investigating the absorption edge shift, the fitting to

Eq. (2) bears significance to long-range fields. Short-range microfields, however, are also likely involved to produce the observed lifetime changes, as will be demonstrated in the following.

Another reason of the uncertainty of the electric field scale arises from a nonuniform field distribution inside the sample. The piezoelectric field distribution $F_{\text{piezo}}(x)$ along the x axis inside a piezoelectric resonator can be attained by solving a standard set of acoustic equations in conjunction with the electromagnetic equations and appropriate mechanical and electrical boundary conditions [22]. If a ratio of the lateral dimensions of a plate to its thickness is large and large surfaces of the plate are fully electroded, the amplitude of the field $F_{\text{piezo}}(x)$ inside the plate for a plate mode with frequency $f_{1,t}^n$ can be approximated by [23]

$$F_{\text{piezo}}(x) = (U/d)\left\{1 + (16Q^2K^4/\pi^2) \times \left[\frac{\sin(\pi f_{1,t}^n d/v_{1,t})}{(\pi f_{1,t}^n d/v_{1,t})} - \cos\frac{2\pi f_{1,t}^n x}{v_{1,t}}\right]^2\right\}^{1/2}, \quad (3)$$

where Q is the quality factor of the chosen mode, K is the electromechanical coupling coefficient and $x = \pm d/2$ correspond to the surfaces of a plate. The plate vibrational modes are essentially standing waves through the thickness of the plate. Therefore, the piezoelectric field oscillates inside a sample at high overtones of plate vibrations so that high- and low-field regions are introduced in the sample interior.

For purposes of the present consideration, it is important to note, however, that the effective value of applied field strength U/d amounts to about 1240 V/cm at $U \approx 70$ V. This value is slightly enhanced in some regions of a plate in accordance with Eq. (3). However, the presented results are not fully applicable to our case of the edge excitation of plate vibrations. Moreover, it seems not unreasonable to assume that remarkably lower piezoelectric fields pervade the platelet interior in our experimental arrangement implying that data have been taken from the sample region which is far apart from the exciting electrodes (see Section 2). Therefore, it seems unlikely that the field scale in Figs. 4 and 7 corresponds to the piezoelectric field strength inside the sample. Hence, the changes of the net charge at crystal defects should be taken into account as already pointed out.

As a thickness of our sample is large enough and an optical absorption of a below band gap laser excitation used turns out to be rather small, effects due to sample surfaces would clearly not dominate the discussed exciton dynamics. Therefore, mention should be made of the electric field of charged point defects and dislocations which are highly nonuniform. To make a dimensional estimate of the field scale presented in Figs. 4 and 7, let us consider the point defect electric fields in the nearest ion distribution [24]. The field strength inside a plate would then be approximated by the normal field

$$F_0 = e/4\pi\varepsilon_0\varepsilon r_0^2, \quad (4)$$

where $(4\pi/3)r_0^3 = 1/N$ is the mean volume per defect, N is the defect concentration, and the other symbols have their usual meaning. Using $N \sim 10^{16}$ cm^{-3} as a typical value of the concentration of defect charges exerted by acoustic driving [12] and $\varepsilon = 9$ for a CdS crystal [17], this readily gives $F_0 \sim 1900$ V/cm.

We hence conclude that the field scale introduced in Figs. 4 and 7 can be reasonably explained in terms of the normal field F_0. However, one should keep in mind that considerable variations in the magnitude of the field strengths occur in the sample interior. It is therefore most likely that electrons and holes released from dissociated excitons above $U \approx 70$ V in the regions of enhanced field strengths migrate to the regions of remarkably lower fields where they can recombine by both through the bound exciton states and donor to acceptor (D^0, A^0) recombination. As the capture probability of charged carriers by D^+ and A^- has been found to be significant [16], the free carrier diffusion away from the regions of considerable field strengths is expected to be accompanied by enhanced donor-to-acceptor recombination, as obviously is the case experimentally in Fig. 2b.

Having validated the electric field approach for the interpretation of our observations, we further proceed with the influence of electric fields on the exciton dynamics. By exploiting the results obtained in Refs. [25,26], the expression given for the

bound exciton lifetime τ is

$$\tau = B/\hbar\omega_{Ex}\xi^3|\psi_0|^2, \quad (5)$$

where B is a constant of proportionality, $\hbar\omega_{Ex}$ is the transition energy, ξ is the range of the wave function for an exciton bound by a short-range potential, and $|\psi_0|^2$ is concerned with the probability of finding an electron and hole on the same site, i.e., the electron–hole wave function overlap. Since the transition energy $\hbar\omega_{Ex}$ does not change appreciably (Fig. 6a), the enhancement of the PL decay time observed in Fig. 4 at $U \leqslant 60$ V can be attributed to an increased electron–hole separation $|\psi_0|^2$ in electric fields exerted by the driving.

The variation of $|\psi_0|^2$ with applied electric field has been numerically elaborated [27]. By applying these results to the electric field range attained in our studies, we have obtained that the enhanced τ should not have been anticipated to exceed ≈ 1.22 ns at $U \approx 60$ V. It is seen in Fig. 4 that the experimentally observed enhancement of the lifetimes is considerably higher. It should be emphasized that the quantitative result of any such comparison with theoretical calculations depends strongly on the particular choice of a field scale in Fig. 4. However, it is important to note that, as illustrated by the above discussion, the scale chosen in Fig. 4 obviously estimates the highest long-range electric fields achieved in our studies. Hence we conclude that the acoustic driving effects lead to a substantial deviation from the estimates made in the long-range electric field approximation.

To interpret the data presented in Fig. 4, we assume that the local field strength at the luminescent center is considerably higher than that presented by the field scale in Figs. 4 and 7. We therefore distinguish between long-range electric fields and short-range microfields generated by the driving. Exactly what sources of the microfields are at issue is a bit subtle. However, there exists a convincing body of empirical evidence in support of the latter possibility. Indeed, studies of deep donors in silicon at acoustic driving have revealed that lattice defects can experience relative displacements in surroundings vibrating at the frequency of external driving [28]. Therefore, changes in the equilibrium positions of defects in a low-frequency vibrating lattice would likely vary the local-crystal environment and generate nonuniform microfields at the bound exciton site. Based on this assumption, the idea appears to be remarkably accurate in describing the lifetime behavior presented in Fig. 4. Indeed, the defect displacements in vibrating surroundings arise from the higher-order terms of the interatomic potential and have been shown to be in square dependence on the amplitude of acoustic driving [28]. This fact is in qualitative agreement with the observations as the increased lifetimes compared to that expected appear only at sufficiently high driving amplitude U, above 20–30 V in Fig. 4.

In support of the assumption made, it should be noted that the threshold field for direct ionization of excitons is simply E_x/ea_x with E_x the exciton binding energy and a_x the effective Bohr radius of the exciton. This field appears to be considerably high in CdS, of the order of 140 kV/cm [27], obviously excluding the possibility of the direct ionization by increased microfields arising from variations in the local-crystal environment within the suggested model. Also of note is that the electric field has been found to produce little effect on the energy of the ground exciton state [27], and this is quite consistent with the fact that no detectable shift of the I_1 exciton line is seen in Fig. 6, spectra 1 and 2.

An additional piece of evidence is derived from the evolution of the PL line shapes presented in Fig. 6. It is well documented that a widening of the exciton trapping potential well ξ can arise from a sufficiently high electric field [27]. Such a broadening is known to broaden PL lines and cause a slight shift of the excitonic level to lower energies which are the case experimentally as spectra 3 in Fig. 6a and b illustrate. Therefore, the reduced exciton lifetimes in Fig. 4 at $U \geqslant 60$ V likely arise from increased ξ in Eq. (5). As both the $|\psi_0|^2$ decrease and the ξ increase occur, an enhancement of the lifetime is initially observed in Fig. 4 with increasing driving amplitude which is followed by a decrease in τ at higher driving amplitudes.

In the picture presented, the effective Bohr radius a_x of the bound exciton would then be anticipated to increase with the assumed decrease of $|\psi_0|^2$. This a_x increase would further lead to the decrease of the

exciton-phonon coupling. Indeed, the probability of the exciton interaction with acoustic phonons is proportional to a form factor [29]

$$f(q) = 1/[1 + (\beta a_x q/2)^2]^2. \quad (6)$$

where q is the phonon wave number, and $\beta = m_h/2(m_e + m_h)$ with m_e and m_h the electron and hole effective mass, respectively. The factor $f(q)$ decreases the exciton coupling to acoustic phonon with increasing exciton radius a_x. An apparent decrease of the acoustic phonon replica I_1–A in spectrum 3 of Fig. 6a can thus be well understood in terms of the presented model. It seems that, obeying essentially the similar dependence (6) the optical phonon replica I_1–LO also tends to decrease in spectrum 3 of Fig. 6b. However, the latter conclusion may not be verifiably justified taking into account a concomitant broadening of spectrum 3 in Fig. 6b which remarkably affects the line shapes of the I_1–LO and I_1–LO–A bands.

In order to directly test our model suggesting the local disturbances at the I_1 exciton site, resonant Raman scattering measurements are employed. It has been established that impurity states modify the group theoretical selection rules because they break the translational and point symmetry [30,31]. This fact is known to enhance the scattering cross-section near the exciton resonance, particularly, at the I_1 bound exciton in CdS [31]. Furthermore, vibrational excitations employed in Raman spectroscopy techniques are known to be very sensitive to the degree of orientational disorder of the crystal structure. Particularly, it has been reported that small amounts of crystal damage or lattice defects can change the momentum conservation law. Enhanced Raman intensities or even normally Raman inactive phonons have consequently been observed in crystals with a lattice disorder [32]. Therefore, to address the question on the short-range interatomic disturbances at the I_1 exciton site accompanying the driving, one can use resonant Raman scattering experiments.

This leads us to the exploitation of the $x(yy)\bar{x}$ scattering orientation signifying the backscattering geometry with the incident laser beam propagating along the x axis and the y axis polarization of the incident and scattered beams. In this geometry, only an E_1 LO phonon [33] is predicted by the momentum conservation law,

$$\boldsymbol{q} = \boldsymbol{k}_i - \boldsymbol{k}_s, \quad (7)$$

where $\boldsymbol{q}(q_x, 0, q_z)$ is the phonon wave vector perpendicular to the y axis, and $\boldsymbol{k}_i(k_x, 0, 0)$ and $\boldsymbol{k}_s(k_x, 0, k_z)$ are the wave vectors of the incident and scattered photons, respectively. By tuning the wavelength of the incident laser light, the enhancement of the LO Raman line near resonance of the I_1 exciton state at about 4888 Å has been observed. Despite almost resonant character of the scattering with 4880 Å laser light presented in Fig. 9, the fundamental conservation law (7) is preserved so that only an E_1 LO phonon is detected in spectrum a of Fig. 9a.

The spectra have been observed to be weakly influenced at $U \leqslant 60$ V and not shown in Fig. 9. While no significant change is obtained for the 2LO phonon line (Fig. 9b), the LO Raman line shape in Fig. 9a exhibits remarkable change at $U \geqslant 60$ V, just on the range of the lifetime decrease observed in Fig. 4.

An important conclusion is that the E_1 phonon line is considerably enhanced in spectrum 2 of Fig. 9a. To explain this observation, consider the resonant contribution to the scattering matrix element R^{ij} for the transitions to a single exciton state of frequency ω_{Ex} which is given by [34]

$$R^{ij} = \frac{1}{V} \frac{p^i_{Ex} \Xi_{Ex} p^j_{Ex}}{(\omega_I - \omega_0 - \omega_{Ex} + i\Gamma)(\omega_I - \omega_{Ex} + i\Gamma)}, \quad (8)$$

where p^i_{Ex} and p^j_{Ex} are the exciton–radiation interaction matrix elements, Ξ_{Ex} is the exciton–lattice matrix element, V is the scattering volume, ω_I is the frequency of the incident laser light, ω_0 is the frequency of the created phonon, Γ is the exciton damping parameter which can be related to the broadness of the exciton state ξ introduced in Eq. (5), and superscripts i and j run over the three Cartesian components.

If the matrix elements $p^{i,j}_{Ex}$ and Ξ_{Ex} are assumed to be independent of the driving amplitude in the absence of the opposite experimental evidence, the enhancement of the E_1 phonon line in Fig. 9a can be attributed to the broadening of the exciton state ξ in Eq. (5). Indeed, the case with 4880 Å (2.541 eV) excitation presented in Fig. 9 is slightly off resonant with the bound exciton state at 4888 Å (2.537 eV).

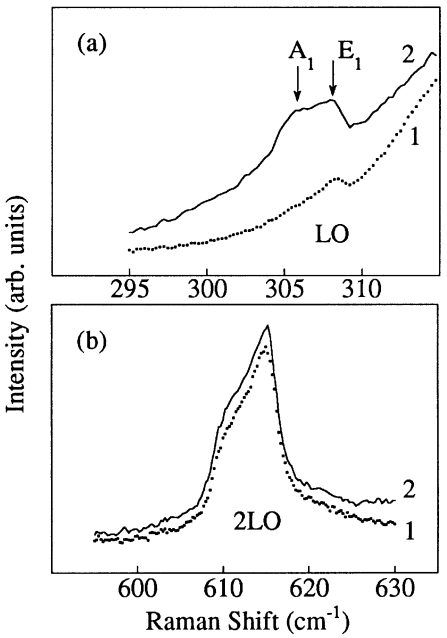

Fig. 9. One (a) and two (b) LO Raman lines at $U = 0$ (1) and $U = 70$ V (2). The background increase in spectra 2 corresponds to the broadening of the I_1–LO (spectrum 3 in Fig. 6b) and I_1–2LO (not shown) luminescence lines for (a) and (b), respectively.

Therefore, the LO phonon line should increase with the broadening because of increased coupling of the incident light ω_I to the Γ-broadened exciton state ω_{Ex} in the second determinator in Eq. (8). By tuning ω_I further enough off the resonance with the I_1 exciton state, no considerable effect of acoustic driving on the Raman scattering has been observed.

The presented observations clearly exclude possible thermal effects that might accompany acoustic driving and influence our data. Indeed, the temperature dependence of R^{ij} in Eq. (8) would come mainly from the variation of ω_{Ex} in the frequency determinators. This being the case, the slight decrease in ω_{Ex} with increasing temperature [35] would be anticipated to vary the scattering cross-section. This is further expected to decrease the strength of the incoming photon resonance satisfying $\omega_I = \omega_{Ex}$ but cannot considerably increase those of the outgoing photon resonance $(\omega_I - \omega_0 = \omega_{Ex})$ which is $\hbar\omega_0 \approx 38$ meV apart from the I_1 line. Accordingly, the decrease of the LO phonon line with temperature increase would be expected to occur which is clearly at variance with the data in Fig. 9a.

Another important conclusion from the data in Fig. 9a is the appearance of an A_1 phonon at $U \geqslant 60$ V which is polarized in the z direction [33]. This appearance stands in contrast with the momentum conservation law (7). This behavior indicates that variations of the local-crystal environment at the exciton site assumed in this work remain to be a reasonable assumption and hence should likewise be in favor of our model of a decrease in the lifetime.

It is worth noting that for two-phonon scattering, the momentum conservation $\boldsymbol{q}_1 + \boldsymbol{q}_2 = \boldsymbol{k}_i - \boldsymbol{k}_s$ is now being driven by both phonons which actually does not restrict the wave vectors of created phonons $\boldsymbol{q}_1$ and $\boldsymbol{q}_2$. Accordingly, all directions of the phonon wave vectors are likely involved in the 2LO Raman scattering process and this is fully consistent with the observation that almost no line shape changes with increasing driving amplitude can be ascertained by analyzing the 2LO Raman lines 1 and 2 presented in Fig. 9b. It is also seen that, in clear contrast to the LO Raman line in Fig. 9a, no intensity change occurs for the 2LO line in Fig. 9b. This observation seems to be a puzzling phenomenon on account of the fact that an expression essentially similar to Eq. (8) can be used for the second-order Raman scattering. It must be pointed out, though, that no resonant enhancement of the 2LO Raman line has been observed by tuning the energy of the incident laser light in the vicinity of the I_1 bound exciton state. Similar effect has been reported in the literature [31] which may be taken to be presumable explanation for the deceptive discrepancy.

5. Conclusions

The experimental evidence is presented that the bound exciton dynamics can be affected by acoustic driving. The changes of the exciton lifetime, photoluminescence intensity and line shape of the PL lines as well as resonant Raman scattering lines have been achieved by acoustically exciting CdS platelets.

The observations are described in terms of the long-range electric fields and nonuniform microfields accompanying acoustic driving. Observed increase in the recombination lifetime is explained by the decrease of the electron–hole wave function overlap whereas the lifetime decrease is indicative of a widening of the exciton state. The suggested model of acoustic driving is confirmed by the driven-induced changes of the resonant Raman scattering. The observed broadening of the PL lines and decrease in emission intensity in the acoustic phonon wing of the I_1 exciton PL line are in reasonable agreement with the proposed mechanism.

At the upper range of the driving amplitudes used in this work the quenching of the exciton PL is observed and it is accompanied by an increased donor-to-acceptor recombination. It is believed that the quenching effect corresponds to the impact ionization of excitons. Free carriers released from the dissociated excitons would then likely diffuse away from the regions of considerable field strengths. Their recapture by ionized donors and acceptors gives rise to the enhanced donor-to-acceptor pair recombination.

Finally, it is important to emphasize that the experiments we designed aimed to show a possibility of attaining the exciton dynamics with the driven internal electric fields. What our results clearly demonstrate is that the ideas of acoustic drivings seem worth extending. Can the size of the effect on the exciton lifetimes be enhanced? Do other bound exciton systems, especially quantum dot structures, show similar effects? Answering these questions will require more experiments.

Acknowledgements

One of us (O.A.K.) thank Dr. M.Y. Shen for his help in measurement techniques. The work was supported by the Ministry of Education, Science, Sports and Culture of Japan.

References

[1] P.J. Dean, D.C. Herbert, in: K. Cho (Ed.), Topics in Current Physics (Excitons), vol. 14, Springer, Berlin, 1979, p. 55.
[2] C.J. Chou, G.F. Neumark, Appl. Phys. Lett. 65 (1994) 761.
[3] R. Benzaquen, R. Leonelli, A.P. Roth, Phys. Rev. B 52 (1995) 1485.
[4] See, e.g., Z.H. Lu, M.C. Hanna, D.M. Szmud, E.G. Oh, A. Majerfild, Appl. Phys. Lett. 56 (1990) 177; P.J. Dean, Prog. Crystal Growth and Charact. 5 (1982) 89; D.C. Reynolds, D.C. Look, D.N. Talwar, G.L. McCoy, K.R. Evans, Phys. Rev. B 51 (1995) 2572.
[5] J. Ding, H. Jeon, T. Ishihara, M. Hagerott, A.V. Nurmikko, H. Luo, N. Samarth, J. Furdyna, Phys. Rev. Lett. 69 (1992) 1707.
[6] H.-J. Polland, L. Schultheis, J. Kuhl, E.O. Göbel, C.W. Tu, Phys. Rev. Lett. 55 (1985) 2610; G. Bastard, E.E. Mendez, L.L. Chang, L. Esaki, Phys. Rev. B 28 (1983) 3241, and references therein.
[7] C. Rocke, S. Zimmermann, A. Wixforth, J.P. Kotthaus, G. Böhm, G. Weimann, Phys. Rev. Lett. 78 (1997) 4099.
[8] K.S. Zhuravlev, D.V. Petrov, Yu.B. Bolkhovityanov, N.S. Rudaja, Appl. Phys. Lett. 70 (1997) 3389.
[9] O.A. Korotchenkov, T. Goto, Appl. Phys. Lett. (1998) in press.
[10] I.V. Ostrovskii, A.Kh. Rozhko, Ukr. Fiz. Zh. (in Russian) 24 (1979) 1404.
[11] I.V. Ostrovskii, P. Das, Appl. Phys. Lett. 70 (1997) 167.
[12] I.V. Ostrovskii, O.A. Korotchenkov, Ukr. Fiz. Zh. (in Russian) 30 (1985) 356; I.V. Ostrovskii, JETP Lett. 34 (1981) 446.
[13] D.G. Thomas, J.J. Hopfield, Phys. Rev. 128 (1962) 2135.
[14] K. Colbow, Phys. Rev. 141 (1966) 742.
[15] A. Migliori, J.L. Sarrao, W.M. Visscher, T.M. Bell, M. Lei, Z. Fisk, R.G. Leisure, Physica B 183 (1993) 1.
[16] J.Y. Lin, D. Baum, Q. Zhu, A. Honig, H.X. Jiang, J. Lumin. 45 (1990) 251.
[17] See, for example, J.I. Pankove, Optical Processes in Semiconductors, Dover, New York, 1975.
[18] Y. Wang, A. Suna, J. McHugh, E.F. Hilinski, P.A. Lucas, R.D. Johnson, J. Chem. Phys. 92 (1990) 6927.
[19] T. Harada, K. Morigaki, J. Phys. Soc. Japan 32 (1972) 172; B.S. Razbirin, I.N. Uraltsev, A.A. Bogdanov, Sov. Phys. Solid State 15 (1973) 604.
[20] D.L. Rode, Phys. Rev. B 2 (1970) 4036.
[21] I.V. Ostrovskii, A.Kh. Rozhko, Sov. Phys. Solid State 26 (1985) 2241.
[22] B.A. Auld, Acoustic Fields and Waves in Solids, vol. II, Krieger Publishing Company, Florida, 1990.
[23] V.N. Lysenko, I.V. Ostrovskii, Sov. Phys. Solid State 23 (1981) 129.
[24] D. Redfield, Phys. Rev. 130 (1963) 916.
[25] E.I. Rashba, G.E. Gurgenishvili, Sov. Phys. Solid State 4 (1962) 759.
[26] C.H. Henry, K. Nassau, Phys. Rev. B 1 (1970) 1628.
[27] D.F. Blossey, Phys. Rev. B 2 (1970) 3976; ibid. 3 (1971) 1382.
[28] O.A. Korotchenkov, H.G. Grimmeiss, Phys. Rev. B 52 (1995) 14598.
[29] A.I. Ansel'm, Yu.A. Firsov, Sov. Phys. JETP 1 (1955) 139; Y. Toyozawa, Prog. Theor. Phys. 20 (1958) 53; T. Bouma,

A.J. Scholten, H.A. Zondag, T.J. Luijendijk, J.I. Dijkhuis, Phys. Rev. B 49 (1994) 1720.
[30] R.M. Martin, T.C. Damen, Phys. Rev. Lett. 26 (1971) 86.
[31] T.C. Damen, J. Shah, Phys. Rev. Lett. 27 (1971) 1506.
[32] D. Powell, A. Compaan, J.R. Macdonald, R.A. Forman, Phys. Rev. B 12 (1975) 20; S. Permogorov, A. Reznitsky, Solid State Commun. 18 (1976) 781.
[33] C.A. Arguello, D.L. Rousseau, S.P.S. Porto, Phys. Rev. 181 (1969) 1351.
[34] R. Loudon, Proc. Roy. Soc. Lond. A 275 (1963) 218; B. Bendow, J.L. Birman, Phys. Rev. B 4 (1971) 569.
[35] C.E. Bleil, J. Phys. Chem. Solids 27 (1966) 1631.